Eur. Phys. J. Plus (2025) 140:858
https://doi.org/10.1140/epjp/s13360-025-06805-z

THE EUROPEAN PHYSICAL JOURNAL PLUS

Regular Article

Simultaneous estimation of three parameters with Heisenberg scaling sensitivity in a two-channel optical network

Atmadev Rai[1], **Danilo Triggiani**[2,3], **Paolo Facchi**[3,4], **Vincenzo Tamma**[1,5,a]

[1] School of Mathematics and Physics, University of Portsmouth, Portsmouth PO1 3HF, UK
[2] Dipartimento Interateneo di Fisica, Politecnico di Bari, 70126 Bari, Italy
[3] INFN, Sezione di Bari, 70126 Bari, Italy
[4] Dipartimento di Fisica, Università di Bari, 70126 Bari, Italy
[5] Institute of Cosmology and Gravitation, University of Portsmouth, Portsmouth PO1 3FX, UK

Received: 24 February 2025 / Accepted: 26 August 2025

Abstract This work presents a quantum sensing interferometric scheme for the simultaneous estimation of multiple parameters at the ultimate quantum scaling precision in a two-mode optical network. This scheme is experimentally feasible because it employs input Gaussian states such as squeezed and coherent states and a relatively low number of experimental runs. We focus on the precise and simultaneous measurement of two unknown phase shifts and an unknown beam splitter reflectivity, achieving Heisenberg scaling sensitivity in all three parameters without any constraints on the parameter values.

1 Introduction

Quantum mechanics has significantly improved the ability for precision measurements in metrology by using quantum properties such as entanglement and squeezing [1–7]. The main benefit of the use of quantum resources is the ability to surpass the classical shot noise limit, where measurement precision typically scales as $1/\sqrt{N}$ with the number of resources N used, such as average number of photons, energy, or time. In contrast, quantum systems can achieve subshot noise scaling up to Heisenberg scaling precision with a scaling of $1/N$ [5, 8–13].

Over the last decade multiparameter estimation has emerged as of significant importance in the field of quantum metrology [14–20]. The simultaneous estimation of multiple physical parameters is gaining attention not only for its potential for resource efficiency, but also for its wide range of applications across various technological fields such as quantum imaging [21–24], biological measurements [25–27], astronomy [28, 29], sensor networks [30, 31], and gravitational wave detection [32, 33]. All these quantum technologies are beyond the single-parameter estimation. Although multiparameter estimation has many applications and has seen recent progress, it still faces major challenges. For instance, using photon number states and entangled states is not easy, both in terms of generating them and maintaining quantum coherence [18, 34]. Moreover, some estimation methods place constraints on the values of unknown parameters, making them unsuitable for use in arbitrarily distributed networks [35–39].

Achieving Heisenberg scaling precision simultaneously in the estimation of multiple parameters consists of multiple uncertainty relations, and the interplay among these multiple uncertainty relations remains largely unexplored. Although much more complex scenarios involving multiple parameters have been theoretically explored in quantum metrology [14, 40–44], and some experiments have also been investigated for multiparameter estimation [45–48], none have yet achieved the ultimate precision for all parameters simultaneously. Therefore, finding the optimal measurement protocols to achieve Heisenberg-limited sensitivity for multiple parameters at the same time still remains a major challenge [49]. In a recent work, Heisenberg scaling is achieved in the simultaneous estimation of two phase parameters of a Mach–Zehnder interferometer [50]. Other two-parameter estimation scenarios have also been explored, including the simultaneous estimation of phase and diffusion noise [51, 52], phase and imperfection in the probe state [53]. However, so far, no scheme has been given for the simultaneous estimation of more than two parameters in an optical network, with Heisenberg scaling using scalable resources such as squeezed states and robust measurement methods such as homodyne detection.

In this article, we introduce a scheme for the estimation of three unknown parameters in a two-mode optical network consisting of two unknown phase shifts and a beam splitter with unknown reflectivity, as shown in Fig. 1, estimating both the phase shifts and the reflectivity simultaneously, and achieving the Heisenberg scaling precision for all three parameters. Our approach involves the injection of a squeezed vacuum and a squeezed-coherent state into the input ports of the optical network, and a measurement with

[a] e-mail: vincenzo.tamma@port.ac.uk (corresponding author)

Published online: 09 September 2025

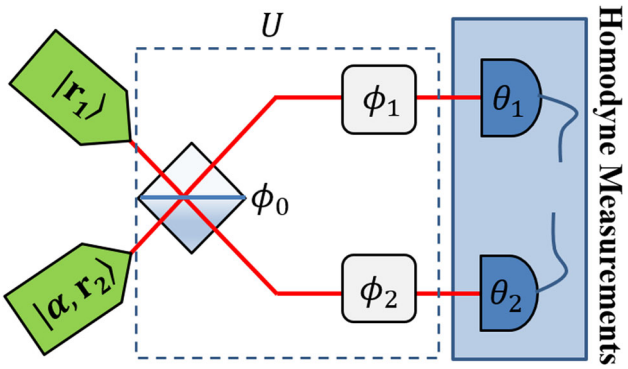

Fig. 1 Experimental scheme for simultaneous estimation of three parameters ϕ_0, ϕ_1 and ϕ_2 in the two-channel network described by the unitary matrix U in Eq. (2). The input probe is initialized using a squeezed vacuum state and a squeezed-coherent state of light, as defined in Eq. (3). Homodyne measurement is performed at both output ports, with local oscillators characterized by phases θ_1 and θ_2

the use of two-homodyne detectors at the output. The advantage of our proposed scheme is that it does not impose any constraints on the values of the unknown parameters, allowing the attainment of Heisenberg scaling in sensitivity, regardless of the values of the parameters. Moreover, our scheme does not require parameter-dependent adaptations within the optical setup, which enhances its practical applicability. We demonstrate that this methodology not only reaches the Heisenberg scaling multiparameter Cramér-Rao bound (CRB) for all three unknown parameters, but is also experimentally scalable.

2 Two channel network

We consider a two-channel linear passive optical network composed of a beam splitter and phase shifters in each arm. In this setup, the beam splitter is characterized by a reflectivity parameter, ϕ_0, while the phase shifts in the upper and lower arms are denoted by ϕ_1 and ϕ_2, respectively, as illustrated in Fig. 1. The operations of the beam splitter (BS) and the phase shifters (PSs) on the optical modes are represented by the unitary matrices

$$\begin{aligned} U_{\rm BS} &= \exp\left(\mathrm{i}\phi_0\sigma_y\right) = \begin{pmatrix} \cos\phi_0 & \sin\phi_0 \\ -\sin\phi_0 & \cos\phi_0 \end{pmatrix}, \\ U_{\rm PS}(\phi_1,\phi_2) &= \begin{pmatrix} e^{\mathrm{i}\phi_1} & 0 \\ 0 & e^{\mathrm{i}\phi_2} \end{pmatrix}, \end{aligned} \tag{1}$$

respectively, where σ_y is the second Pauli matrix. Therefore, the overall optical network, as depicted in Fig. 1, can be described by the unitary matrix

$$U = U_{\rm PS}U_{\rm BS} = (\sqrt{p_{ij}}e^{\mathrm{i}\gamma_{ij}})_{ij} = \begin{pmatrix} e^{\mathrm{i}\phi_1}\cos\phi_0 & e^{\mathrm{i}\phi_1}\sin\phi_0 \\ -e^{\mathrm{i}\phi_2}\sin\phi_0 & e^{\mathrm{i}\phi_2}\cos\phi_0 \end{pmatrix}. \tag{2}$$

The elements of this unitary matrix are expressed as $U_{ij} = \sqrt{p_{ij}}e^{\mathrm{i}\gamma_{ij}}$, where $p_{ij} = |U_{ij}|^2$ with $i,\ j = 1,\ 2$ represents the transition probability of a photon from input channel j to output channel i within the interferometer, and $\gamma_{ij} = \mathrm{Arg}[U_{ij}]$ is the corresponding phase shift experienced by the photon. Given that U is a 2×2 unitary matrix, it follows that $p_{11} = p_{22} = p_1$ and $p_{12} = p_{21} = p_2$.

Here, we propose an estimation scheme which aims to achieve Heisenberg scaling precision in the simultaneous estimation of three unknown parameters, particularly the two phase shifts ϕ_1, ϕ_2 and the BS reflectivity ϕ_0. As depicted in Fig. 1, the input probe we consider in our scheme is given by

$$|\psi\rangle_{\rm in} = |r_1\rangle \otimes |\alpha, r_2\rangle, \tag{3}$$

where $|r_1\rangle$ is a squeezed vacuum state with an average photon number $N_{s1} = \sinh^2(r_1)$, and $|\alpha,\ r_2\rangle$ is a displaced squeezed state with an average photon number $N_c + N_{s2} = |\alpha|^2 + \sinh^2(r_2)$, injected into the first and second input ports, respectively. Here, $r_{1,2}$ are the real squeezing parameters, and $|\alpha|$ represents the amplitude of the coherent light.

At the final step, we perform balanced homodyne detections at both output ports to measure the quadratures $\hat{x}_{i,\theta_i}$ (for $i = 1,\ 2$), where θ_i is the phase of the local oscillator associated with the i-th homodyne detector. From these measurements, the unknown parameters $\boldsymbol{\phi} = (\phi_0,\ \phi_1,\ \phi_2)$ can be inferred. The joint probability distribution function associated with the outcomes of homodyne measurements follows a Gaussian distribution

$$p_{\boldsymbol{\phi}}(\vec{x}) = \frac{1}{2\pi\sqrt{\mathrm{Det}[\Sigma]}}\exp\left[-\frac{(\vec{x}-\vec{\mu})^T\Sigma^{-1}(\vec{x}-\vec{\mu})}{2}\right], \tag{4}$$

where Σ is the covariance matrix and $\vec{\mu}$ is the mean vector, both of which depends on the unknown parameters ϕ_0, ϕ_1 and ϕ_2 through the interferometric transformation of the input state. Detailed expressions for the first and second moments of the output state can be found in Appendix A. Given that both output ports are measured and probes are injected into both input ports, all elements of the

unitary matrix U described in Eq. (2) become relevant. The mean vector $\vec{\mu}$ and the elements of the covariance matrix Σ for equal squeezing ($r_1 = r_2 = r$), in terms of the phases of the two local oscillators, reads

$$\vec{\mu} = \sqrt{2}\alpha \begin{pmatrix} \sin\phi_0 \sin(\theta_1 - \phi_1) \\ \cos\phi_0 \sin(\theta_2 - \phi_2) \end{pmatrix}, \tag{5}$$

and

$$\begin{aligned} \Sigma_{11} &= \frac{1}{2}[\cosh 2r + \cos 2(\phi_1 - \theta_1)\sinh 2r], \\ \Sigma_{22} &= \frac{1}{2}[\cosh 2r + \cos 2(\phi_2 - \theta_2)\sinh 2r], \\ \Sigma_{12} &= \Sigma_{21} = 0. \end{aligned} \tag{6}$$

3 Multiparameter Fisher information matrix

In our optical setup, multiple unknown parameters are involved; therefore, our theoretical analysis of the precision in their estimation needs to make use of a multiparameter formalism. The Fisher information matrix (FIM) describes the precision in the estimation of multiple parameters [54]. It quantifies the amount of information a given measurement can extract about the unknown parameters to be estimated. Here, we compute the FIM for the simultaneous estimation of the reflectivity of the BS ϕ_0 and the two phase shifts ϕ_1 and ϕ_2 using homodyne detection at the output ports of the optical network in Fig. 1. The FIM establishes a lower bound on the estimation error, commonly known as the CRB, given by

$$\mathrm{Cov}[\tilde{\boldsymbol{\phi}}] \geq \frac{1}{\nu} F^{-1}[\boldsymbol{\phi}], \tag{7}$$

where ν is the number of independent measurements, F represents the positive semi-definite FIM, and $\mathrm{Cov}[\tilde{\boldsymbol{\phi}}]$ refers to the covariance matrix of the estimators $\tilde{\boldsymbol{\phi}} = (\tilde{\phi}_0, \tilde{\phi}_1, \tilde{\phi}_2)$ of the parameters $\boldsymbol{\phi} = (\phi_0, \phi_1, \phi_2)$. By utilizing the probability distribution given in Eq. (4), we derive the elements of the FIM as shown in Appendix B. These elements can be written as:

$$F_{mn} = \underbrace{\partial_{\phi_m}\vec{\mu}^T \Sigma^{-1}\partial_{\phi_n}\vec{\mu}}_{\mathrm{F}^{\mathcal{S}}_{mn}} + \underbrace{\frac{1}{2}\mathrm{Tr}\big[\Sigma^{-1}(\partial_{\phi_m}\Sigma)\Sigma^{-1}(\partial_{\phi_n}\Sigma)\big]}_{\mathrm{F}^{\mathcal{N}}_{mn}}, \tag{8}$$

for $m, n \in \{0, 1, 2\}$, where $\mathrm{Tr}[\cdot]$ denotes the trace operation. The FIM in Eq. (8) decomposes into the sum of two terms, $F^{\mathcal{S}}$ and $F^{\mathcal{N}}$, representing respectively the contribution from the *signal* and the *noise* of the outcome of homodyne measurements.

To proceed further, we define the total average number of photons in the squeezed inputs as $N_s = N_{s1} + N_{s2}$, and the total photon number in both the input ports as $N = N_c + N_s$. In the following section, we demonstrate that under the assumption $N_{c,s} = O(N)$, it is possible to achieve a precision at the Heisenberg scaling, $O(1/N)$, in estimating all three parameters ϕ_0, ϕ_1, and ϕ_2 without requiring any adaptation of the optical system. This scaling is achieved after we impose that the local oscillator phases of the homodyne detection are experimentally tuned values of θ_1 and θ_2 of the asymptotic form

$$\theta_i = \gamma_i + \frac{k_i}{N_{s_i}}, \quad i = 1, 2, \tag{9}$$

where $\gamma_i = \gamma_{ii} \pm \frac{\pi}{2}$ specifies the phases of the quadrature fields $\hat{x}_{i,\gamma_i}$ at which the minimum variance is observed. In other words, the local oscillator phases are detuned from γ_i by an additional term k_i/N_{s_i}, where k_i is an arbitrary constant independent of N_s.

In the following section, we show that the Fisher information related to the variation of noise, $F^{\mathcal{N}}$, in Eq. (8), is sufficient to achieve Heisenberg scaling precision for the estimation of the two unknown phases ϕ_1 and ϕ_2. Additionally, by exploiting the information contained in the variation of the signal, $F^{\mathcal{S}}$, we demonstrate that it is eventually possible to estimate also the BS reflectivity parameter ϕ_0 with Heisenberg scaling.

4 Three-parameter estimation

In this section, we focus on the simultaneous estimation of the three parameters $\boldsymbol{\phi} = (\phi_0, \phi_1, \phi_2)$ using the homodyne measurement outcomes described earlier. As the FIM have contributions from both the signal and noise in Eq. (8), we will analyze these two contributions separately. First, we obtain the information associated with the variation of the noise given by the second term $F^{\mathcal{N}}$ in the FIM 8 by substituting Σ^{-1} and the derivatives of Σ with respect to the parameters using Eq. (6), and we find that the only nonzero elements of matrix $F^{\mathcal{N}}$ are the diagonal ones

$$F_{22}^{\mathcal{N}} = \frac{2N_s(N_s+2)\sin[2(\phi_1-\theta_1)]^2}{1+N_s+\sqrt{N_s}\sqrt{N_s+2}\cos[2(\phi_1-\theta_1)]^2},$$
$$F_{33}^{\mathcal{N}} = \frac{2N_s(N_s+2)\sin[2(\phi_2-\theta_2)]^2}{1+N_s+\sqrt{N_s}\sqrt{N_s+2}\cos[2(\phi_2-\theta_2)]^2}. \tag{10}$$

To achieve Heisenberg scaling in the CRB of parameters, ϕ_1 and ϕ_2 both elements in Eq. (10) must be of the order N_s^2, which can be reached by tuning the local oscillators in the homodyne detections according to the condition 9 with the minimum variance phase γ_i of the measured quadrature field $\hat{x}_i$, with $i = 1, 2$. For a large number of photons, $F^{\mathcal{N}}$ asymptotically reads

$$F^{\mathcal{N}} = \begin{pmatrix} 0 & 0 & 0 \\ 0 & \frac{128k_1^2N_s^2}{(1+16k_1^2)^2} & 0 \\ 0 & 0 & \frac{128k_2^2N_s^2}{(1+16k_2^2)^2} \end{pmatrix}. \tag{11}$$

Now, we analyze the first contribution to the FIM 8, which is the information extracted from the variation of the displacement $\vec{\mu}$ with respect to the parameters. By choosing $k_1 = k_2 = k$ in the condition 9, $F^{\mathcal{S}}$ asymptotically reads (see Appendix C)

$$F^{\mathcal{S}} = \begin{pmatrix} \frac{8N_cN_s}{1+16k^2} & 0 & 0 \\ 0 & 0 & 0 \\ 0 & 0 & 0 \end{pmatrix} \tag{12}$$

where all orders smaller than $O(N^2)$, which do not contribute to the Heisenberg scaling, are neglected. To estimate all three parameters ϕ_0, ϕ_1, and ϕ_2 simultaneously at the Heisenberg-limited sensitivity, we consider the total FIM $F = F^{\mathcal{S}} + F^{\mathcal{N}}$ in Eqs. (11) and (12):

$$F = \begin{pmatrix} \frac{8N_cN_s}{1+16k^2} & 0 & 0 \\ 0 & \frac{128k^2N_s^2}{(1+16k^2)^2} & 0 \\ 0 & 0 & \frac{128k^2N_s^2}{(1+16k^2)^2} \end{pmatrix}. \tag{13}$$

The CRB in Eq. (7) then reads

$$(\Delta\phi_0)^2 \geq (\Delta\phi_0^{CRB})^2 = \frac{1}{\nu}\frac{(1+16k^2)}{8N_cN_s}, \tag{14}$$

$$(\Delta\phi_1)^2 \geq (\Delta\phi_1^{CRB})^2 = \frac{1}{\nu}\frac{(1+16k^2)^2}{128k^2N_s^2}, \tag{15}$$

$$(\Delta\phi_2)^2 \geq (\Delta\phi_2^{CRB})^2 = \frac{1}{\nu}\frac{(1+16k^2)^2}{128k^2N_s^2}, \tag{16}$$

and gives the Heisenberg scaling in all three parameters simultaneously. The FIM F in Eq. (13) is diagonal to leading order in $O(N^2)$, implying that each of the three parameters can be estimated with the Heisenberg scaling precision independently. In other words, achieving Heisenberg scaling for one parameter does not affect the estimation of the others. We also observe that for $k = 1/4$, the prefactors for the uncertainties of both ϕ_1 and ϕ_2 are minimized.

This demonstrates that the precision for estimating all three parameters achieves Heisenberg scaling in the asymptotic limit. In particular, the estimation of the parameters ϕ_1 and ϕ_2 reaches this scaling with a precision of $\Delta\phi_{1(2)} = O(1/N_s)$, regardless of the intensity of the coherent state, as it depends solely on the number of squeezed photons. On the other hand, the estimation of ϕ_0 also achieves the Heisenberg scaling provided that the average photon numbers in both the coherent state (N_c) and the squeezed state (N_s) are proportional to the total average photon number $N = N_s + N_c$. The precision is optimal when $N_c = N_s = N/2$, i.e., when averagely half of the input photons are coherent and half are squeezed, yielding $\Delta\phi_0 = O(1/N)$. We note that in our model, the two squeezed inputs remain separable after the beam splitter, resulting in the output covariance matrix Σ being independent of the beam splitter reflectivity ϕ_0 and depends only on the phases ϕ_1 and ϕ_2. Consequently, the Fisher term $F^{\mathcal{N}}$, which arises from variation of Σ, encodes solely the phase shift information, whereas the term $F^{\mathcal{S}}$, originating from derivatives of the mean vector $\vec{\mu}$, allows the estimation of the reflectivity ϕ_0 with Heisenberg scaling.

The Cramér-Rao bounds in Eqs. (14)–(16) are asymptotically saturated through the use of maximum likelihood estimators, thus achieving the desired Heisenberg scaling precision. The analytical form of the maximum likelihood estimators (MLEs) for parameters ϕ_0, ϕ_1 and ϕ_2 is

$$\tilde{\phi}_{0\,\mathrm{MLE}} = \arctan\left[\frac{-\tilde{\mu}_1}{\tilde{\mu}_2}\right], \tag{17}$$

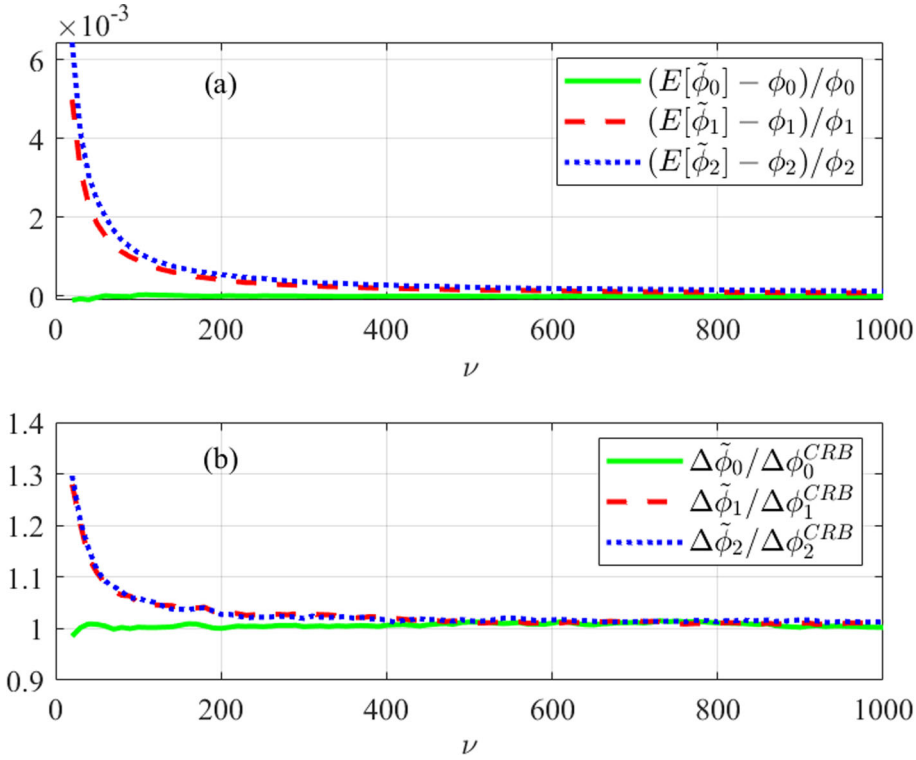

Fig. 2 Maximum likelihood estimation of parameters ϕ_0 (green continuous line), ϕ_1 (red dashed line), and ϕ_2 (blue dotted line) as a function of the number of measurements ν. (a) Relative bias and (b) saturation of the CRB for the estimated parameters obtained from the maximum likelihood estimation. We notice in panel (a) that $\tilde{\phi}_0$ is already unbiased for a very small number of experimental iterations ν (see appendix E). The CRB in Eqs. (15) and (16) is saturated, reaching already a ratio $\Delta\tilde{\phi}_i/\Delta\phi_i{}^{CRB}$ close to 1.05 (i.e., within 5% of the CRB) for number of experimental iterations $\nu = 100$ and saturates the bounds for a number of repetitions of the measurement already of the order of 500. The CRB for $\tilde{\phi}_0$ is already saturated for even a very small number of iterations ν (see appendix F). Here, we take the values of $\phi_{0,1,2} = \pi/5$, $\pi/3$, $\pi/4$, $|\alpha|^2 = 5$ and $N_s = 5$

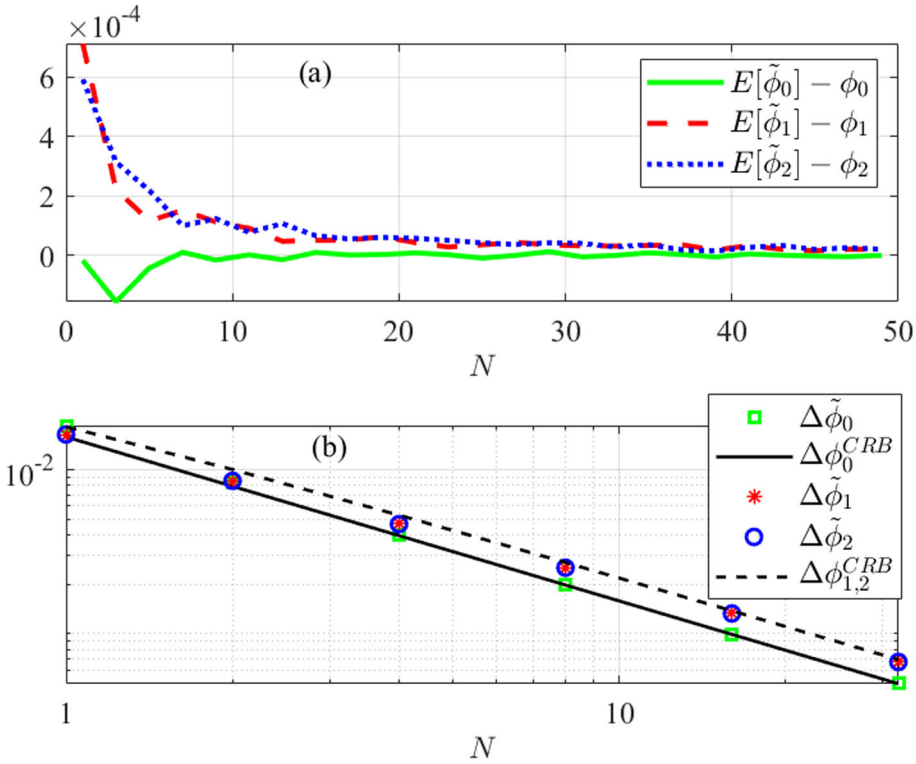

Fig. 3 Maximum likelihood estimation of the parameters ϕ_0, ϕ_1 and ϕ_2 as a function of total number of photons N, with equal average number of squeezed and coherent photons, $N_c = N_s = N/2$. (a) Bias in the estimated parameters ϕ_0 (green continuous line), ϕ_1 (red dashed line), and ϕ_2 (blue dotted line); (b) Heisenberg scaling in the uncertainty for all the parameters, $\Delta\phi_i = O(1/N)$ with $i = 1, 2, 3$. In (b), the uncertainty in the estimation of ϕ_0 (green squares), ϕ_1 (red asterisks) and ϕ_2 (blue circles) are compared with the CRBs of ϕ_0 (black continuous line) and $\phi_{1,2}$ (black dashed line) derived in Eqs. (14)–(16), for $k = 1/4$. The uncertainties $\Delta\tilde{\phi}_i$ in the estimator $\tilde{\phi}_i$ approach the CRB already for a relatively small number N of photons. Here, we take the value of $\phi_{0,1,2} = \pi/3$, $\pi/7$, $\pi/8$, and the sample size $\nu = 1000$

$$\tilde{\phi}_{1\,\mathrm{MLE}} = \theta_1 + \frac{1}{2}\left[-2\pi + \arccos\left(\frac{2\tilde{\Sigma}_{11} - \cosh 2r}{\sinh 2r}\right)\right], \tag{18}$$

$$\tilde{\phi}_{2\,\mathrm{MLE}} = \theta_2 + \frac{1}{2}\left[-4\pi + \arccos\left(\frac{2\tilde{\Sigma}_{22} - \cosh 2r}{\sinh 2r}\right)\right], \tag{19}$$

and a detailed calculation is provided in Appendix D. In Figs. 2 and 3, the precision of such estimators is analyzed in terms of the number of probe photons and experimental repetitions. In particular, Fig. 2(a) plots the relative bias $(\mathbb{E}[\tilde{\phi}_i] - \phi_i)/\phi_i$ for each parameter as a function of the measurement repetitions, where $\mathbb{E}[\tilde{\phi}_i]$ is the expected value of the estimator $\tilde{\phi}_i$, and ϕ_i is the true value of the parameter, with $i = 0, 1, 2$. Figure 3(a) shows the bias as a function of the average photon number N. Figures 2(b) and 3(b) depict the uncertainties $\Delta\phi_i$ in comparison with the CRBs.

The results demonstrate that the estimators $\tilde{\phi}_1$ and $\tilde{\phi}_2$ are asymptotically unbiased and achieve the CRB with Heisenberg scaling for a number of measurement repetitions already of the order of 500. Notably, the estimator $\tilde{\phi}_0$ is approximately unbiased for even very small iterations and average number of photons (see Appendix E for a detailed calculation). The bias of $\tilde{\phi}_0$ is approximately zero up to $O(1/\nu^2 N^4)$ which remains negligible even for a relatively very small average number of input photons. (See the solid green plot in Figs. 2(a)and 3(a)). Furthermore, the variance of the estimator $\tilde{\phi}_0$ asymptotically matches the CRB of the parameter ϕ_0 in Eq. (14) up to first error correction term of $O(1/\nu^3 N^6)$, which is negligible even for very small values average number of photons, saturating the CRB as shown in Figs. 2b and 3b (see Appendix F).

5 Conclusions

In this paper, we have presented a scheme that simultaneously estimates three unknown parameters with ultimate Heisenberg scaling precision in a two-channel optical network, which is illuminated by both squeezed light and squeezed-coherent light sources at the input. Homodyne measurements at both output ports allow us to reach the ultimate scaling irrespective of the values of the parameters, and our scheme does not need any adaptation of the network. We show that the Heisenberg scaling of two phase parameters, ϕ_1 and ϕ_2, is only given by the variation of the noise of the measurement, whereas the unknown reflectivity ϕ_0 is extracted only from the variation of the signal of the homodyne measurement. We also show that the CRBs are parameter-independent functions. Additionally, we have demonstrated that the maximum likelihood estimator reaches the theoretical CRB with only a number of experimental iterations of order 500, making the scheme experimentally feasible. While our analysis is based on the CRB and employs maximum likelihood estimation, which is well-known to be effective in the asymptotic regime, alternative global and Bayesian methods have been developed to address the inherent limitations of the CRB approach [53, 55–58]. Interestingly, the parameter ϕ_0 shows an unbiased behavior and saturates the CRB already for very small average number of photons in the channel. Achieving the ultimate quantum sensitivity in the estimation of three parameters simultaneously opens a new frontier in quantum optical metrology. Recently, large optical squeezing has been demonstrated [59]. Although our scheme achieves three-parameter Heisenberg scaling sensitivity in a lossless optical network, investigating the effects of losses and detector inefficiencies remains an interesting direction for future work [60, 61].

Acknowledgements This project is partially supported by Xairos Systems Inc. VT also acknowledges partial support from the Air Force Office of Scientific Research under award number FA8655-23-17046. PF was partially supported by Istituto Nazionale di Fisica Nucleare (INFN) through the project "QUANTUM," by the Italian National Group of Mathematical Physics (GNFM-INdAM), and by the Italian funding within the "Budget MUR - Dipartimenti di Eccellenza 2023–2027" - Quantum Sensing and Modelling for One-Health (QuaSiModO). D.T. acknowledges the Italian Space Agency (ASI, Agenzia Spaziale Italiana) through the project Subdiffraction Quantum Imaging (SQI) n. 2023-13-HH.0.

Data Availability Statement This manuscript has no associated data.

Appendix A Details of balanced Homodyne measurement outcomes

Here, we will derive the expressions for the mean vector $\vec{\mu}$ and the covariance matrix Σ, presented in Eqs. (5) and (6), respectively, associated with the outcomes of the homodyne measurements.

We can describe a 2-mode Gaussian state using its Wigner distribution function, defined as

$$W(\mathbf{z}) = \frac{1}{(2\pi)^2\sqrt{\det\Gamma}}\exp\left[-\frac{1}{2}(\mathbf{z}-\mathbf{d})^T\Gamma^{-1}(\mathbf{z}-\mathbf{d})\right], \quad \mathbf{z}\in\mathbb{R}^4, \tag{A1}$$

where $\mathbf{d}$ is the displacement vector and Γ is the covariance matrix of the input state $|r_1\rangle\otimes|\alpha, r_2\rangle$ in Eq. (3). Here, r_1 and r_2 are the real squeezing parameters and $\alpha = |\alpha|e^{i\pi/2}$ is a complex displacement amplitude. The covariance matrix and displacement vector in phase space are given by

$$\Gamma = \tfrac{1}{2}\mathrm{diag}(e^{2r_1}, e^{2r_2}, e^{-2r_1}, e^{-2r_2}), \quad \mathbf{d} = \sqrt{2}\,(0,0,0,|\alpha|)^T. \tag{A2}$$

The Wigner distribution $W(\mathbf{z})$ of the state $\hat{U}|r_1\rangle \otimes |\alpha, r_2\rangle$ after applying $\hat{U}$ obtained by rotating the initial Wigner distribution with the orthogonal and symplectic matrix R associated with the unitary matrix U reads

$$R = \begin{pmatrix} \mathrm{Re}[U] & -\mathrm{Im}[U] \\ \mathrm{Im}[U] & \mathrm{Re}[U] \end{pmatrix}, \tag{A3}$$

so that

$$\Gamma_U = R\,\Gamma\,R^T, \quad \mathbf{d}_U = R\,\mathbf{d}. \tag{A4}$$

Finally, balanced homodyne detection with local oscillator phases $\theta_{1,2}$ projects onto quadratures $\hat{x}_{i,\theta_i}$. This can be implemented by applying an additional unitary rotation $U(\theta) = \mathrm{diag}(e^{-i\theta_1}, e^{-i\theta_2})$ to the state $\hat{U}|r_1\rangle \otimes |\alpha, r_2\rangle$, which introduces a phase $e^{-i\theta_i}$ to each element of the i-th row of U. Thus, the elements of the overall unitary matrix can be written as $\sqrt{p_{ij}}e^{i(\gamma_{ij}-\theta_i)}$, where $\gamma_{ij} = \arg[U_{ij}]$ for $i,\ j = 1, 2$. The resulting joint outcome of the homodyne detection is a Gaussian distribution characterized by a mean vector and a covariance matrix. The mean $\vec{\mu}$ corresponds to the first two elements of the transformed displacement vector $\mathbf{d}_U$, given by

$$\vec{\mu} = \sqrt{2}|\alpha|\begin{pmatrix} -\sqrt{p_2}\sin(\gamma_{12}-\theta_1) \\ -\sqrt{p_1}\sin(\gamma_{22}-\theta_2) \end{pmatrix}, \tag{A5}$$

and covariance matrix Σ given by the upper 2×2 block of Γ_U. Its components are explicitly given by:

$$\begin{aligned}
\Sigma_{11} &= \frac{1}{2}\big[p_1(\cosh 2r_1 + \cos 2(\gamma_{11}-\theta_1)\sinh 2r_1) + p_2(\cosh 2r_2 + \cos 2(\gamma_{12}-\theta_1)\sinh 2r_2)\big], \\
\Sigma_{22} &= \frac{1}{2}\big[p_2(\cosh 2r_1 + \cos 2(\gamma_{21}-\theta_2)\sinh 2r_1) + p_1(\cosh 2r_2 + \cos 2(\gamma_{22}-\theta_2)\sinh 2r_2)\big], \\
\Sigma_{12} = \Sigma_{21} &= \frac{\sqrt{p_1 p_2}}{2}\big[\cos(\gamma_{11}-\gamma_{21}-\theta_1+\theta_2)\cosh 2r_1 + \cos(\gamma_{11}+\gamma_{21}-\theta_1-\theta_2)\sinh 2r_1 \\
&\quad + \cos(\gamma_{12}-\gamma_{22}-\theta_1+\theta_2)\cosh 2r_2 + \cos(\gamma_{12}+\gamma_{22}-\theta_1-\theta_2)\sinh 2r_2\big].
\end{aligned} \tag{A6}$$

For the unitary matrix in Eq. (2) and equal input squeezings $r_1 = r_2 = r$, the expressions for $\vec{\mu}$ and Σ in Eqs. (A5) and (A6) reduce respectively to Eqs. (5) and (6) of the main text.

Appendix B Deriving the Fisher information matrix for Gaussian probability in Eq. (8)

In this appendix, for completeness, we derive the well-known FIM of a multivariate Gaussian distribution based on the joint probability distribution of homodyne measurements [62]. In general, the FIM is defined by [54]

$$F_{mn} = \mathbb{E}_{p_{\boldsymbol{\phi}}}\big[\big(\partial_{\phi_m}\log p_{\boldsymbol{\phi}}(\vec{x})\big)\big(\partial_{\phi_n}\log p_{\boldsymbol{\phi}}(\vec{x})\big)\big]. \tag{B1}$$

To compute the FIM, we first evaluate the logarithmic derivatives of $p_{\boldsymbol{\phi}}(\vec{x})$ given by

$$p_{\boldsymbol{\phi}}(\vec{x}) = \frac{1}{2\pi\sqrt{\mathrm{Det}[\Sigma]}}\exp\left[-\frac{(\vec{x}-\vec{\mu})^T\Sigma^{-1}(\vec{x}-\vec{\mu})}{2}\right], \tag{B2}$$

where the mean vector $\vec{\mu}$ and the covariance matrix Σ are functions of the parameters $\boldsymbol{\phi} = (\phi_0, \phi_1, \phi_2)$. This requires using the properties of Gaussian integrals, which allow us to simplify the expectation values of polynomial terms involving $(\vec{x}-\vec{\mu})$ up to fourth order:

$$\begin{aligned}
\mathbb{E}_{p_{\boldsymbol{\phi}}}[(x_i-\mu_i)] &= 0, \\
\mathbb{E}_{p_{\boldsymbol{\phi}}}\big[(x_i-\mu_i)(x_j-\mu_j)\big] &= \Sigma_{ij}, \\
\mathbb{E}_{p_{\boldsymbol{\phi}}}\big[(x_i-\mu_i)(x_j-\mu_j)(x_k-\mu_k)\big] &= 0, \\
\mathbb{E}_{p_{\boldsymbol{\phi}}}\big[(x_i-\mu_i)(x_j-\mu_j)(x_k-\mu_k)(x_l-\mu_l)\big] &= \Sigma_{ij}\Sigma_{kl} + \Sigma_{ik}\Sigma_{jl} + \Sigma_{il}\Sigma_{jk}.
\end{aligned} \tag{B3}$$

Substituting these results into the expression for F_{mn} yields

$$\begin{aligned}
F_{mn} &= \frac{1}{4}\big(\partial_{\phi_m}\log\mathrm{Det}[\Sigma]\big)\big(\partial_{\phi_n}\log\mathrm{Det}[\Sigma]\big) \\
&\quad + \sum_{i,j=1}^{2}\Big((\partial_{\phi_m}\vec{\mu}^T)\Sigma^{-1}\Big)_i\Big((\partial_{\phi_n}\vec{\mu}^T)\Sigma^{-1}\Big)_j\mathbb{E}_{p_{\boldsymbol{\phi}}}\big[(x_i-\mu_i)(x_j-\mu_j)\big] \\
&\quad + \frac{1}{4}\big(\partial_{\phi_m}\log\mathrm{Det}[\Sigma]\big)\sum_{i,j=1}^{2}(\partial_{\phi_n}\Sigma^{-1}_{ij})\mathbb{E}_{p_{\boldsymbol{\phi}}}\big[(x_i-\mu_i)(x_j-\mu_j)\big]
\end{aligned}$$

$$+\frac{1}{4}\left(\partial_{\phi_n}\log\mathrm{Det}[\Sigma]\right)\sum_{i,j=1}^{2}(\partial_{\phi_m}\Sigma_{ij}^{-1})\mathbb{E}_{p_{\boldsymbol{\phi}}}\left[(x_i-\mu_i)(x_j-\mu_j)\right]$$

$$+\frac{1}{4}\sum_{i,j,k,l=1}^{2}(\partial_{\phi_m}\Sigma_{ij}^{-1})(\partial_{\phi_n}\Sigma_{kl}^{-1})\mathbb{E}_{p_{\boldsymbol{\phi}}}\left[(x_i-\mu_i)(x_j-\mu_j)(x_k-\mu_k)(x_l-\mu_l)\right]. \tag{B4}$$

Using Jacobi's formula for the derivative of the determinant of a matrix

$$\frac{\partial_{\phi_i}\mathrm{Det}[\Sigma]}{\mathrm{Det}[\Sigma]}=\mathrm{Tr}\left[\Sigma^{-1}\partial_{\phi_i}\Sigma\right]=-\mathrm{Tr}\left[\partial_{\phi_i}\Sigma^{-1}\Sigma\right], \tag{B5}$$

we simplify Eq. (B4) as

$$F_{mn}=\underbrace{\partial_{\phi_m}\vec{\mu}^{T}\Sigma^{-1}\partial_{\phi_n}\vec{\mu}}_{\mathrm{F}^{\mathcal{S}}_{mn}}+\underbrace{\frac{1}{2}\mathrm{Tr}\left[\Sigma^{-1}(\partial_{\phi_m}\Sigma)\Sigma^{-1}(\partial_{\phi_n}\Sigma)\right]}_{\mathrm{F}^{\mathcal{N}}_{mn}}, \tag{B6}$$

Here, the first term $F^{\mathcal{S}}$ tells how the mean of the homodyne outcome $\vec{\mu}$ changes with the change in parameters, while the second term $F^{\mathcal{N}}$ arises from the derivatives of the covariance matrix Σ, which quantifies how the parameters affect the fluctuations of the measurement outcome. The total FIM gives the complete information of the parameters encoded in a general Gaussian state.

Appendix C Evaluation of $F^{\mathcal{S}}$ in equation (12)

To evaluate the value of $F^{\mathcal{S}}$ in Eq. (12), we first calculate the derivatives of $\vec{\mu}$ in Eq. (5) with respect to parameters ϕ_0, ϕ_1 and ϕ_2:

$$\begin{aligned}
\partial_{\phi_0}\vec{\mu}&=\sqrt{2}\alpha\begin{pmatrix}\cos\phi_0\sin(\theta_1-\phi_1)\\-\sin\phi_0\sin(\theta_2-\phi_2)\end{pmatrix},\\
\partial_{\phi_1}\vec{\mu}&=\sqrt{2}\alpha\begin{pmatrix}-\sin\phi_0\cos(\theta_1-\phi_1)\\0\end{pmatrix},\\
\partial_{\phi_2}\vec{\mu}&=\sqrt{2}\alpha\begin{pmatrix}0\\-\cos\phi_0\cos(\theta_2-\phi_2)\end{pmatrix}.
\end{aligned} \tag{C1}$$

By substituting the inverse of the covariance matrix Σ in Eq. (6) and the derivatives of μ in Eq. (C1) into Eq. (8), $F^{\mathcal{S}}$ reads

$$\begin{pmatrix}
\frac{4N_c\cos^2(\phi_0)\sin^2(\phi_1-\theta_1)}{1+N_s+\sqrt{N_s}\sqrt{N_s+2}\cos[2(\phi_1-\theta_1)]}+\frac{4N_c\sin^2(\omega)\sin^2(\phi_2-\theta_2)}{1+N_s+\sqrt{N_s}\sqrt{N_s+2}\cos[2(\phi_2-\theta_2)]} & \frac{N_c\sin(2\phi_0)\sin[2(\phi_1-\theta_1)]}{1+N_s+\sqrt{N_s}\sqrt{N_s+2}\cos[2(\phi_1-\theta_1)]} & \frac{-N_c\sin(2\phi_0)\sin[2(\phi_2-\theta_2)]}{1+N_s+\sqrt{N_s}\sqrt{N_s+2}\cos[2(\phi_2-\theta_2)]}\\
\frac{4N_c\sin^2(\omega)\sin^2(\phi_2-\theta_2)}{1+N_s+\sqrt{N_s}\sqrt{N_s+2}\cos[2(\phi_1-\theta_1)]} & \frac{4N_c\sin^2(\phi_0)\cos^2(\phi_1-\theta_1)}{1+N_s+\sqrt{N_s}\sqrt{N_s+2}\cos[2(\phi_1-\theta_1)]} & 0\\
\frac{-N_c\sin(2\phi_0)\sin[2(\phi_2-\theta_2)]}{1+N_s+\sqrt{N_s}\sqrt{N_s+2}\cos[2(\phi_2-\theta_2)]} & 0 & \frac{4N_c\cos^2(\phi_0)\cos^2(\phi_2-\theta_2)}{1+N_s+\sqrt{N_s}\sqrt{N_s+2}\cos[2(\phi_2-\theta_2)]}
\end{pmatrix} \tag{C2}$$

After using the condition on the local oscillator in (9) and for a symmetric case, say $k_1=k_2=k$, $F^{\mathcal{S}}$ can be written asymptotically as

$$F^{\mathcal{S}}=\begin{pmatrix}
\frac{8N_cN_s}{1+16k^2}+O(N) & \frac{8kN_c\sin(2\phi_0)}{1+16k^2}+O(N^0) & \frac{-8kN_c\sin(2\phi_0)}{1+16k^2}+O(N^0)\\
\frac{8kN_c\sin(2\phi_0)}{1+16k^2}+O(N^0) & \frac{32k^2N_c\sin^2(\phi_0)}{N_s(1+16k^2)} & 0\\
\frac{-8kN_c\sin(2\phi_0)}{1+16k^2}+O(N^0) & 0 & \frac{32k^2N_c\cos^2(\phi_0)}{N_s(1+16k^2)}
\end{pmatrix} \tag{C3}$$

and reduce to Eq. (12) up to $O(N^2)$.

Appendix D Maximum Likelihood Estimators

In this appendix, we find the maximum likelihood estimators (MLEs) saturating the CRBs as given in Eq. (7). Consider ν repeated independent measurements using two-homodyne detection of the quadratures $\hat{x}_{i,\theta_i}$, giving a set of outcomes $\{\vec{x}_1,\ldots,\vec{x}_\nu\}$. The likelihood function is expressed as

$$L(\boldsymbol{\phi}|\vec{x}_1,...,\vec{x}_\nu)=\prod_{i=1}^{\nu}p(\vec{x}_i|\boldsymbol{\phi}), \tag{D1}$$

where $p(\vec{x}_i|\boldsymbol{\phi})$ represents the probability density function associated with the joint homodyne measurement described in Eq. (4). To find the MLE $\tilde{\boldsymbol{\phi}}$, we maximize the log-likelihood function $\log(L)$, and obtain

$$\begin{aligned}
0 &= \nabla_{\boldsymbol{\phi}} \log L(\boldsymbol{\phi}|\vec{x}_1, ..., \vec{x}_\nu)\Big|_{\boldsymbol{\phi}=\tilde{\boldsymbol{\phi}}_{MLE}} \\
&= \nabla_{\boldsymbol{\phi}} \sum_{i=1}^{\nu} \log p(\vec{x}_i|\boldsymbol{\phi})\Big|_{\boldsymbol{\phi}=\tilde{\boldsymbol{\phi}}_{MLE}} \\
&= \Big[-\frac{\nu}{2}\nabla_{\boldsymbol{\phi}} \log(\det[\Sigma]) - \frac{1}{2}\nabla_{\boldsymbol{\phi}} \sum_{i=1}^{\nu} (\vec{x}_i - \vec{\mu})^T \Sigma^{-1} (\vec{x}_i - \vec{\mu}) \Big]_{\boldsymbol{\phi}=\tilde{\boldsymbol{\phi}}_{MLE}} \\
&= \Big[-\frac{\nu}{2}\mathrm{Tr}\big[\Sigma^{-1}\nabla_{\boldsymbol{\phi}}\Sigma\big] - \frac{1}{2}\nabla_{\boldsymbol{\phi}} \sum_{i=1}^{\nu} \mathrm{Tr}\big[\Sigma^{-1}(\vec{x}_i - \vec{\mu})(\vec{x}_i - \vec{\mu})^T\big] \Big]_{\boldsymbol{\phi}=\tilde{\boldsymbol{\phi}}_{MLE}} \\
&= \Big[(\nabla_{\boldsymbol{\phi}}\vec{\mu})^T \Sigma^{-1} \Big(\nu\vec{\mu} - \sum_{i=1}^{\nu} \vec{x}_i \Big) \Big]_{\boldsymbol{\phi}=\tilde{\boldsymbol{\phi}}_{MLE}} + \frac{1}{2}\mathrm{Tr}\Big[\nabla_{\boldsymbol{\phi}}\Sigma^{-1} \Big(\nu\Sigma - \sum_{i=1}^{\nu} (\vec{x}_i - \vec{\mu})(\vec{x}_i - \vec{\mu})^T \Big) \Big]_{\boldsymbol{\phi}=\tilde{\boldsymbol{\phi}}_{MLE}} .
\end{aligned} \tag{D2}$$

Note that Eq. (D2) leads to three separate equations, corresponding to the derivatives with respect to ϕ_0, ϕ_1 and ϕ_2. In general, these equations are not analytically solvable. However, in the case discussed in the main text when squeezed amplitudes are equal, the equations simplify, and the covariance matrix Σ becomes independent of ϕ_0, and therefore the derivative with respect to ϕ_0 reduces to

$$0 = \Big[(\nabla_{\phi_0}\vec{\mu})^T \Sigma^{-1} \Big(\nu\vec{\mu} - \sum_{i=1}^{\nu} \vec{x}_i \Big) \Big]_{\phi_0=\tilde{\phi}_0^{MLE}}, \tag{D3}$$

which gives the estimator $\tilde{\vec{\mu}} = \frac{1}{\nu}\sum_{i=1}^{\nu} \vec{x}_i$ for the mean $\vec{\mu}$. By utilizing Eqs. (5) along with the local oscillator conditions in Eq. (9), where $k_1 = k_2$, this further simplifies as

$$\frac{\mu_1}{\mu_2} = \frac{\tilde{\mu}_1}{\tilde{\mu}_2} \Rightarrow -\frac{\sin\tilde{\phi}_0}{\cos\tilde{\phi}_0} = \frac{\tilde{\mu}_1}{\tilde{\mu}_2}, \tag{D4}$$

leading to an explicit expression for the MLE of ϕ_0 in Eq. (17) in the main text

$$\tilde{\phi}_{0\,\mathrm{MLE}} = \arctan\Big[-\frac{\tilde{\mu}_1}{\tilde{\mu}_2} \Big]. \tag{D5}$$

However for the parameters ϕ_1 and ϕ_2, both terms in Eq. (D2) in general contribute to the solution. Considering the asymptotic behavior for large N, we find that under the local oscillator condition (9) $\partial_{\phi_{1(2)}}\vec{\mu} = O(N^0)$, $\partial_{\phi_{1(2)}}\Sigma^{-1} = O(N^2)$, $\Sigma^{-1} = O(N)$, $\Sigma = O(N)$, and $\vec{\mu}$ grows as $O(N^{1/2})$. Consequently, the first term of Eq. (D2) scales as $O(N)$, while the second term is of order $O(N^2)$. Thus, for large N, second term dominant and Eq. (D2) can be written as

$$0 = \frac{1}{2}\mathrm{Tr}\Big[\nabla_{\boldsymbol{\phi}}\Sigma^{-1} \Big(\nu\Sigma - \sum_{i=1}^{\nu} (\vec{x}_i - \vec{\mu})(\vec{x}_i - \vec{\mu})^T \Big) \Big]_{\boldsymbol{\phi}=\tilde{\boldsymbol{\phi}}_{MLE}} . \tag{D6}$$

This can be solved and provide the sample covariance matrix

$$\tilde{\Sigma} = \frac{1}{\nu}\sum_{i=1}^{\nu} (\vec{x}_i - \tilde{\vec{\mu}})(\vec{x}_i - \tilde{\vec{\mu}})^T, \tag{D7}$$

which is an estimator for the actual covariance matrix Σ. Substituting this into the above equation and equating the result to the diagonal matrix Σ in Eq. (6), we obtain the maximum likelihood estimators for ϕ_1 and ϕ_2 in Eqs. (18) and (19) in the main text, given by

$$\tilde{\phi}_{1\,\mathrm{MLE}} = \theta_1 + \frac{1}{2}\Big[-2\pi + \arccos\Big(\frac{2\tilde{\Sigma}_{11} - \cosh 2r}{\sinh 2r} \Big) \Big], \tag{D8}$$

$$\tilde{\phi}_{2\,\mathrm{MLE}} = \theta_2 + \frac{1}{2}\Big[-4\pi + \arccos\Big(\frac{2\tilde{\Sigma}_{22} - \cosh 2r}{\sinh 2r} \Big) \Big], \tag{D9}$$

where $\tilde{\Sigma}_{ij}$ are the entries of the matrix $\tilde{\Sigma}$. It is worth noting that the estimators $\tilde{\phi}_1$ and $\tilde{\phi}_2$ in Eqs. (18) and (19) give a good approximation to the solutions of Eq. (D2), even for smaller values of N, also shown in Fig. 2 and Fig. 3 of the main text.

Appendix E Unbiasness of estimator $\tilde{\phi}_0$

In this appendix, we aim to show that the MLE $\tilde{\phi}_0 = \arctan\left[-\tilde{\mu}_1/\tilde{\mu}_2\right]$ in Eq. (17) is approximately an unbiased estimator of the parameter $\phi_0 = \arctan\left[-\mu_1/\mu_2\right]$, if the higher-order terms are negligible, where $\tilde{\mu}_1$ and $\tilde{\mu}_2$ are the sample means of bivariate normal distribution and μ_1 and μ_2 are the means of the marginal distribution.

We know that the sample means $\tilde{\mu}_1$ and $\tilde{\mu}_2$ are unbiased estimators of the population means μ_1 and μ_2, respectively. To analyze the unbiasedness of $\tilde{\phi}_0$, we begin by expanding $f(\tilde{\mu}_1, \tilde{\mu}_2) = \arctan[-\tilde{\mu}_1/\tilde{\mu}_2]$ around (μ_1, μ_2) using a Taylor series expansion

$$\begin{aligned} f(\tilde{\mu}_1, \tilde{\mu}_2) =& f(\mu_1, \mu_2) + \frac{\partial f}{\partial \tilde{\mu}_1}\bigg|_{\mu_1,\mu_2} (\tilde{\mu}_1 - \mu_1) + \frac{\partial f}{\partial \tilde{\mu}_2}\bigg|_{\mu_1,\mu_2} (\tilde{\mu}_2 - \mu_2) + \frac{1}{2}\frac{\partial^2 f}{\partial \tilde{\mu}_1^2}\bigg|_{\mu_1,\mu_2} (\tilde{\mu}_1 - \mu_1)^2 \\ &+ \frac{1}{2}\frac{\partial^2 f}{\partial \tilde{\mu}_2^2}\bigg|_{\mu_1,\mu_2} (\tilde{\mu}_2 - \mu_2)^2 + \frac{\partial^2 f}{\partial \tilde{\mu}_1 \partial \tilde{\mu}_2}\bigg|_{\mu_1,\mu_2} (\tilde{\mu}_1 - \mu_1)(\tilde{\mu}_2 - \mu_2) + \text{higher-order terms}. \end{aligned} \tag{E1}$$

Taking the expectation of the above expression, we get

$$\begin{aligned} \mathbb{E}[f(\tilde{\mu}_1, \tilde{\mu}_2)] =& f(\mu_1, \mu_2) + \frac{\partial f}{\partial \tilde{\mu}_1}\bigg|_{\mu_1,\mu_2} \mathbb{E}[\tilde{\mu}_1 - \mu_1] + \frac{\partial f}{\partial \tilde{\mu}_2}\bigg|_{\mu_1,\mu_2} \mathbb{E}[\tilde{\mu}_2 - \mu_2] + \frac{1}{2}\frac{\partial^2 f}{\partial \tilde{\mu}_1^2}\bigg|_{\mu_1,\mu_2} \mathbb{E}[(\tilde{\mu}_1 - \mu_1)^2] \\ &+ \frac{1}{2}\frac{\partial^2 f}{\partial \tilde{\mu}_2^2}\bigg|_{\mu_1,\mu_2} \mathbb{E}[(\tilde{\mu}_2 - \mu_2)^2] + \frac{\partial^2 f}{\partial \tilde{\mu}_1 \partial \tilde{\mu}_2}\bigg|_{\mu_1,\mu_2} \mathbb{E}[(\tilde{\mu}_1 - \mu_1)(\tilde{\mu}_2 - \mu_2)] + \mathbb{E}[\text{higher-order terms}]. \end{aligned} \tag{E2}$$

Since $\tilde{\mu}_1$ and $\tilde{\mu}_2$ are unbiased estimators, $\mathbb{E}[\tilde{\mu}_1 - \mu_1] = 0$ and $\mathbb{E}[\tilde{\mu}_2 - \mu_2] = 0$, the first-order correction term vanishes, leading to $\mathbb{E}[\tilde{\phi}_0] \approx \arctan[-\mu_1/\mu_2] = \phi_0$. This shows that $\tilde{\phi}_0$ is an unbiased estimator to first order. Furthermore Eq. (E2) can be written as

$$\begin{aligned} \mathbb{E}[\tilde{\phi}_0] =& \phi_0 + \frac{\mu_1\mu_2}{(\mu_1^2+\mu_2^2)^2}\text{Var}[\tilde{\mu}_1] - \frac{\mu_1\mu_2}{(\mu_1^2+\mu_2^2)^2}\text{Var}[\tilde{\mu}_2] \\ &+ \frac{\mu_1^2-\mu_2^2}{(\mu_1^2+\mu_2^2)^2}\text{Cov}[\tilde{\mu}_1, \tilde{\mu}_2] + \mathbb{E}[\text{higher-order terms}] \end{aligned} \tag{E3}$$

where $\text{Var}[\tilde{\mu}_1]$ and $\text{Var}[\tilde{\mu}_2]$ are the variances and $\text{Cov}[\tilde{\mu}_1, \tilde{\mu}_2]$ is the covariance of the sample mean $\tilde{\mu}_1$ and $\tilde{\mu}_2$ and are directly related to the population variance Σ in Eq. (6) for a sample size ν, reads

$$\text{Var}[\tilde{\mu}_1] = \frac{\Sigma_{11}}{\nu},\ \text{Var}[\tilde{\mu}_2] = \frac{\Sigma_{22}}{\nu}, \text{and } \text{Cov}[\tilde{\mu}_1, \tilde{\mu}_2] = \frac{\Sigma_{12}}{\nu}. \tag{E4}$$

By substituting μ_1, μ_2 and Σ from Eqs. (5) and (6), using the condition (9), into Eq. (E3), we can express $\mathbb{E}[\tilde{\phi}_0]$ as

$$\mathbb{E}[\tilde{\phi}_0] = \phi_0 + \frac{(C_2 - C_1)\sin(2\phi_0)}{4\nu N_c N_s} + O(\frac{1}{\nu^2 N^4}) + \ldots \approx \phi_0, \tag{E5}$$

where $C_{1(2)} = (16k_{1(2)} + 1)^2/4$. For the the case $k_1 = k_2 = k$, the bias $\mathbb{E}[\tilde{\phi}_0] - \phi_0 = O(1/\nu^2 N^4)$ vanishes rapidly with increasing ν and N, and implies that the MLE $\tilde{\phi}_0$ is unbiased since the error term $O(1/\nu^2 N^4)$ is negligible. In particular, Figs. 2(a) and 3(a) show $\tilde{\phi}_0$ is unbiased for a very small number of iterations ν and small average photons N.

Appendix F Variance of the estimator $\tilde{\phi}_0$

Here, we will show that the CRB of the estimator $\tilde{\phi}_0$ is approximately saturated even for very small iterations and a small average number of photons. To evaluate the asymptotic behavior of the CRB of $\tilde{\phi}_0$, we first calculate the variance $(\Delta\tilde{\phi}_0)^2$, given by

$$\begin{aligned} (\Delta\tilde{\phi}_0)^2 &= \mathbb{E}[\tilde{\phi}_0^2] - \mathbb{E}[\tilde{\phi}_0]^2 \\ &= \mathbb{E}[\Big(\arctan\left[-\frac{\tilde{\mu}_1}{\tilde{\mu}_2}\right]\Big)^2] - \mathbb{E}[\arctan\left[-\frac{\tilde{\mu}_1}{\tilde{\mu}_2}\right]]^2 \\ &= \Big(\arctan\left[\frac{\mu_1}{\mu_2}\right]^2 + \frac{\mu_2(\mu_2 - 2\mu_1\arctan[\mu_1/\mu_2])\text{Var}[\tilde{\mu}_1]}{(\mu_1^2+\mu_2^2)^2} + \frac{\mu_1(\mu_1 + 2\mu_2\arctan[\mu_1/\mu_2])\text{Var}[\tilde{\mu}_2]}{(\mu_1^2+\mu_2^2)^2} + \\ &\frac{-2\mu_1\mu_2 + 2(\mu_1^2-\mu_2^2)\arctan[\mu_1/\mu_2])\text{Cov}[\tilde{\mu}_1, \tilde{\mu}_2]}{(\mu_1^2+\mu_2^2)^2} + \mathbb{E}[\text{higher-order terms}]\Big) - \\ &\Big(\arctan\left[-\frac{\mu_1}{\mu_2}\right] + \frac{\mu_1\mu_2\text{Var}[\tilde{\mu}_1]}{(\mu_1^2+\mu_2^2)^2} - \frac{\mu_1\mu_2\text{Var}[\tilde{\mu}_2]}{(\mu_1^2+\mu_2^2)^2} + \frac{\mu_1^2-\mu_2^2\text{Cov}[\tilde{\mu}_1, \tilde{\mu}_2]}{(\mu_1^2+\mu_2^2)^2} + \mathbb{E}[\text{higher-order terms}]\Big)^2. \end{aligned} \tag{F1}$$

Similar to the above calculation of $\mathbb{E}[\tilde{\phi}]$ in Appendix E, by substituting μ_1, μ_2, and Σ from Eqs. (5) and (6) and using the condition (9), we can derive an asymptotic form of the variance $(\Delta\tilde{\phi}_0)^2$, which reads

$$(\Delta\tilde{\phi}_0)^2 = \frac{(C_1 + C_2) + (C_1 - C_2)\cos(2\phi_0)}{4\nu N_c N_s} - \frac{(C_1 - C_2)\sin^2(2\phi_0)}{16\nu^2 N_c^2 N_s^2} + O(1/\nu^3 N^6) + \dots. \tag{F2}$$

Here, we can see that even the term $O(1/\nu^2 N^4)$ is very small and the estimator is efficient neglecting $O(1/\nu^2 N^4)$. For the case $k_1 = k_2 = k$, $(\Delta\tilde{\phi}_0)^2$ can be written as

$$(\Delta\tilde{\phi}_0)^2 = \frac{1}{\nu}\frac{16k^2+1}{8N_c N_s} + O(1/\nu^3 N^6) + \ldots \approx \frac{1}{\nu}\frac{16k^2+1}{8N_c N_s}; \tag{F3}$$

this expression is the CRB of the parameter ϕ_0 given in Eq. (14) in the main text. The asymptotic variance $(\Delta\tilde{\phi}_0)^2$ confirms that the MLE for parameter ϕ_0 saturates its CRB, since the higher-order error terms are negligible even for a very small number of iterations ν and small average number of photons N, as shown in Figs. 2b and 3b.

References

1. V. Giovannetti, S. Lloyd, L. Maccone, Quantum metrology. Phys. Rev. Lett. **96**, 010401 (2006). https://doi.org/10.1103/PhysRevLett.96.010401
2. M.G. Paris, Quantum estimation for quantum technology. Int. J. Quant. Inf. **7**(supp01), 125–137 (2009)
3. V. Giovannetti, S. Lloyd, L. Maccone, Advances in quantum metrology. Nat. Photonics **5**(4), 222–229 (2011)
4. R. Schnabel, Squeezed states of light and their applications in laser interferometers. Phys. Rep. **684**, 1–51 (2017)
5. C.M. Caves, Quantum-mechanical noise in an interferometer. Phys. Rev. D **23**, 1693–1708 (1981). https://doi.org/10.1103/PhysRevD.23.1693
6. L. Pezzé, A. Smerzi, Mach-Zehnder interferometry at the Heisenberg limit with coherent and squeezed-vacuum light. Phys. Rev. Lett. **100**, 073601 (2008). https://doi.org/10.1103/PhysRevLett.100.073601
7. M.D. Lang, C.M. Caves, Optimal quantum-enhanced interferometry using a laser power source. Phys. Rev. Lett. **111**, 173601 (2013). https://doi.org/10.1103/PhysRevLett.111.173601
8. D. Triggiani, P. Facchi, V. Tamma, Non-adaptive Heisenberg-limited metrology with multi-channel homodyne measurements. Europ. Phys. J. Plus **137**(1), 1–13 (2022)
9. G. Gramegna, D. Triggiani, P. Facchi, F.A. Narducci, V. Tamma, Heisenberg scaling precision in multi-mode distributed quantum metrology. New J. Phys. **23**(5), 053002 (2021). https://doi.org/10.1088/1367-2630/abf67f
10. G. Gramegna, D. Triggiani, P. Facchi, F.A. Narducci, V. Tamma, Typicality of Heisenberg scaling precision in multimode quantum metrology. Phys. Rev. Res. **3**, 013152 (2021). https://doi.org/10.1103/PhysRevResearch.3.013152
11. J.P. Dowling, K.P. Seshadreesan, Quantum optical technologies for metrology, sensing, and imaging. J. Lightwave Technol. **33**(12), 2359–2370 (2015)
12. S. Zhou, M. Zhang, J. Preskill, L. Jiang, Achieving the Heisenberg limit in quantum metrology using quantum error correction. Nat. Commun. **9**(1), 78 (2018)
13. K. Qian, Z. Eldredge, W. Ge, G. Pagano, C. Monroe, J.V. Porto, A.V. Gorshkov, Heisenberg-scaling measurement protocol for analytic functions with quantum sensor networks. Phys. Rev. A **100**(4), 042304 (2019)
14. P.C. Humphreys, M. Barbieri, A. Datta, I.A. Walmsley, Quantum enhanced multiple phase estimation. Phys. Rev. Lett. **111**, 070403 (2013). https://doi.org/10.1103/PhysRevLett.111.070403
15. J.-D. Yue, Y.-R. Zhang, H. Fan, Quantum-enhanced metrology for multiple phase estimation with noise. Sci. Rep. **4**(1), 5933 (2014)
16. L.B. Ho, H. Hakoshima, Y. Matsuzaki, M. Matsuzaki, Y. Kondo, Multiparameter quantum estimation under dephasing noise. Phys. Rev. A **102**, 022602 (2020). https://doi.org/10.1103/PhysRevA.102.022602
17. Y. Yao, L. Ge, X. Xiao, X. Wang, C.P. Sun, Multiple phase estimation for arbitrary pure states under white noise. Phys. Rev. A **90**, 062113 (2014). https://doi.org/10.1103/PhysRevA.90.062113
18. S. Hong, J. Ur Rehman, Y.-S. Kim, Y.-W. Cho, S.-W. Lee, H. Jung, S. Moon, S.-W. Han, H.-T. Lim, Quantum enhanced multiple-phase estimation with multi-mode n 00 n states. Nat. Commun. **12**(1), 5211 (2021)
19. C.N. Gagatsos, D. Branford, A. Datta, Gaussian systems for quantum-enhanced multiple phase estimation. Phys. Rev. A **94**, 042342 (2016). https://doi.org/10.1103/PhysRevA.94.042342
20. L. Pezzè, M.A. Ciampini, N. Spagnolo, P.C. Humphreys, A. Datta, I.A. Walmsley, M. Barbieri, F. Sciarrino, A. Smerzi, Optimal measurements for simultaneous quantum estimation of multiple phases. Phys. Rev. Lett. **119**, 130504 (2017). https://doi.org/10.1103/PhysRevLett.119.130504
21. M.I. Kolobov, Quantum Limits of Optical Super-Resolution, pp. 113–139. Springer, New York, NY (2007). https://doi.org/10.1007/0-387-33988-4_6
22. N. Spagnolo, L. Aparo, C. Vitelli, A. Crespi, R. Ramponi, R. Osellame, P. Mataloni, F. Sciarrino, Quantum interferometry with three-dimensional geometry. Sci. Rep. **2**(1), 862 (2012)
23. M. Genovese, Real applications of quantum imaging. J. Opt. **18**(7), 073002 (2016). https://doi.org/10.1088/2040-8978/18/7/073002
24. C. Napoli, S. Piano, R. Leach, G. Adesso, T. Tufarelli, Towards superresolution surface metrology: quantum estimation of angular and axial separations. Phys. Rev. Lett. **122**, 140505 (2019). https://doi.org/10.1103/PhysRevLett.122.140505
25. M.A. Taylor, J. Janousek, V. Daria, J. Knittel, B. Hage, H.-A. Bachor, W.P. Bowen, Biological measurement beyond the quantum limit. Nat. Photonics **7**(3), 229–233 (2013)
26. M.A. Taylor, W.P. Bowen, Quantum metrology and its application in biology. Phys. Rep. **615**, 1–59 (2016)
27. N. Mauranyapin, L. Madsen, M. Taylor, M. Waleed, W. Bowen, Evanescent single-molecule biosensing with quantum-limited precision. Nat. Photonics **11**(8), 477–481 (2017)
28. S.Z. Ang, R. Nair, M. Tsang, Quantum limit for two-dimensional resolution of two incoherent optical point sources. Phys. Rev. A **95**, 063847 (2017). https://doi.org/10.1103/PhysRevA.95.063847
29. b. Řehaček, Z. Hradil, B. Stoklasa, M. Paúr, J. Grover, A. Krzic, L.L. Sánchez-Soto, Multiparameter quantum metrology of incoherent point sources: Towards realistic superresolution. Phys. Rev. A **96**, 062107 (2017). https://doi.org/10.1103/PhysRevA.96.062107
30. P. Komar, E.M. Kessler, M. Bishof, L. Jiang, A.S. Sørensen, J. Ye, M.D. Lukin, A quantum network of clocks. Nat. Phys. **10**(8), 582–587 (2014)
31. J. Nokkala, F. Arzani, F. Galve, R. Zambrini, S. Maniscalco, J. Piilo, N. Treps, V. Parigi, Reconfigurable optical implementation of quantum complex networks. New J. Phys. **20**(5), 053024 (2018)

32. A. Freise, S. Chelkowski, S. Hild, W. Pozzo, A. Perreca, A. Vecchio, Triple michelson interferometer for a third-generation gravitational wave detector. Class. Quantum Gravity **26**(8), 085012 (2009)
33. R. Schnabel, N. Mavalvala, D.E. McClelland, P.K. Lam, Quantum metrology for gravitational wave astronomy. Nat. Commun. **1**(1), 121 (2010)
34. F. Yao, Y.-M. Du, H. Xing, L. Fu, Two-parameter estimation with three-mode noon state in a symmetric triple-well potential. Commun. Theor. Phys. **74**(4), 045103 (2022)
35. X. Guo, C.R. Breum, J. Borregaard, S. Izumi, M.V. Larsen, T. Gehring, M. Christandl, J.S. Neergaard-Nielsen, U.L. Andersen, Distributed quantum sensing in a continuous-variable entangled network. Nat. Phys. **16**(3), 281–284 (2020)
36. Q. Zhuang, J. Preskill, L. Jiang, Distributed quantum sensing enhanced by continuous-variable error correction. New J. Phys. **22**(2), 022001 (2020)
37. Q. Zhuang, Z. Zhang, Physical-layer supervised learning assisted by an entangled sensor network. Phys. Rev. X **9**, 041023 (2019). https://doi.org/10.1103/PhysRevX.9.041023
38. D. Gatto, P. Facchi, F.A. Narducci, V. Tamma, Distributed quantum metrology with a single squeezed-vacuum source. Phys. Rev. Res. **1**, 032024 (2019). https://doi.org/10.1103/PhysRevResearch.1.032024
39. D. Gatto, P. Facchi, V. Tamma, Heisenberg-limited estimation robust to photon losses in a Mach-Zehnder network with squeezed light. Phys. Rev. A **105**, 012607 (2022). https://doi.org/10.1103/PhysRevA.105.012607
40. H. Imai, A. Fujiwara, Geometry of optimal estimation scheme for su (d) channels. J. Phys. A: Math. Theor. **40**(16), 4391 (2007)
41. T. Baumgratz, A. Datta, Quantum enhanced estimation of a multidimensional field. Phys. Rev. Lett. **116**, 030801 (2016). https://doi.org/10.1103/PhysRevLett.116.030801
42. M. Szczykulska, T. Baumgratz, A. Datta, Multi-parameter quantum metrology. Adv. Phys.: X **1**(4), 621–639 (2016)
43. S. Ragy, M. Jarzyna, R. Demkowicz-Dobrzański, Compatibility in multiparameter quantum metrology. Phys. Rev. A **94**, 052108 (2016). https://doi.org/10.1103/PhysRevA.94.052108
44. D. Triggiani, P. Facchi, V. Tamma, Heisenberg scaling precision in the estimation of functions of parameters in linear optical networks. Phys. Rev. A **104**, 062603 (2021). https://doi.org/10.1103/PhysRevA.104.062603
45. E. Polino, M. Riva, M. Valeri, R. Silvestri, G. Corrielli, A. Crespi, N. Spagnolo, R. Osellame, F. Sciarrino, Experimental multiphase estimation on a chip. Optica **6**(3), 288–295 (2019)
46. Z. Hou, H. Zhu, G.-Y. Xiang, C.-F. Li, G.-C. Guo, Achieving quantum precision limit in adaptive qubit state tomography. NPJ Quantum Inf. **2**(1), 1–5 (2016)
47. P.M. Birchall, E.J. Allen, T.M. Stace, J.L. O'Brien, J.C.F. Matthews, H. Cable, Quantum optical metrology of correlated phase and loss. Phys. Rev. Lett. **124**, 140501 (2020). https://doi.org/10.1103/PhysRevLett.124.140501
48. E. Roccia, I. Gianani, L. Mancino, M. Sbroscia, F. Somma, M.G. Genoni, M. Barbieri, Entangling measurements for multiparameter estimation with two qubits. Quant. Sci. Technol. **3**(1), 01–01 (2017)
49. E. Polino, M. Valeri, N. Spagnolo, F. Sciarrino, Photonic quantum metrology. AVS Quantum Science **2**(2) (2020)
50. A. Rai, D. Triggiani, P. Facchi, V. Tamma, Heisenberg-limited sensitivity in the estimation of two parameters in a mach-zehnder interferometer. arXiv preprint arXiv:2405.17115 (2024)
51. M.D. Vidrighin, G. Donati, M.G. Genoni, X.-M. Jin, W.S. Kolthammer, M. Kim, A. Datta, M. Barbieri, I.A. Walmsley, Joint estimation of phase and phase diffusion for quantum metrology. Nat. Commun. **5**(1), 3532 (2014)
52. M. Altorio, M.G. Genoni, M.D. Vidrighin, F. Somma, M. Barbieri, Weak measurements and the joint estimation of phase and phase diffusion. Phys. Rev. A **92**, 032114 (2015). https://doi.org/10.1103/PhysRevA.92.032114
53. E. Roccia, V. Cimini, M. Sbroscia, I. Gianani, L. Ruggiero, L. Mancino, M.G. Genoni, M.A. Ricci, M. Barbieri, Multiparameter approach to quantum phase estimation with limited visibility. Optica **5**(10), 1171–1176 (2018). https://doi.org/10.1364/OPTICA.5.001171
54. H. Cramér, *Mathematical Methods of Statistics*, vol. 9 (Princeton University Press, Princeton, NJ, 1999)
55. M. Valeri, E. Polino, D. Poderini, I. Gianani, G. Corrielli, A. Crespi, R. Osellame, N. Spagnolo, F. Sciarrino, Experimental adaptive Bayesian estimation of multiple phases with limited data. NPJ Quant. Inf. **6**(1), 92 (2020)
56. J. Rubio, P.A. Knott, T.J. Proctor, J.A. Dunningham, Quantum sensing networks for the estimation of linear functions. J. Phys. A: Math. Theor. **53**(34), 344001 (2020)
57. K.K. Lee, C. Gagatsos, S. Guha, A. Ashok, Quantum multi-parameter adaptive bayesian estimation and application to super-resolution imaging. arXiv preprint arXiv:2202.09980 (2022)
58. B. Liu, K.-X. Yang, Y.-L. Mao, L. Feng, B. Guo, S. Xu, H. Chen, Z.-D. Li, J. Fan, Experimental adaptive Bayesian estimation for a linear function of distributed phases in photonic quantum networks. Optica **11**(10), 1419–1424 (2024). https://doi.org/10.1364/OPTICA.532865
59. H. Vahlbruch, M. Mehmet, K. Danzmann, R. Schnabel, Detection of 15 DB squeezed states of light and their application for the absolute calibration of photoelectric quantum efficiency. Phys. Rev. Lett. **117**, 110801 (2016). https://doi.org/10.1103/PhysRevLett.117.110801
60. R. Demkowicz-Dobrzanski, U. Dorner, B.J. Smith, J.S. Lundeen, W. Wasilewski, K. Banaszek, I.A. Walmsley, Quantum phase estimation with lossy interferometers. Phys. Rev. A **80**, 013825 (2009). https://doi.org/10.1103/PhysRevA.80.013825
61. G. Frascella, S. Agne, F.Y. Khalili, M.V. Chekhova, Overcoming detection loss and noise in squeezing-based optical sensing. NPJ Quantum Inf. **7**(1), 72 (2021)
62. S.M. Kay, *Fundamentals of statistical processing, volume I: estimation theory* (Prentice Hall PTR, Upper Saddle River, NJ, 1993)